Geomechanics for Energy and the Environment 15 (2018) 54–64

Contents lists available at ScienceDirect

Geomechanics for Energy and the Environment

journal homepage: www.elsevier.com/locate/gete

Theoretical and experimental investigations on the role of transient effects in the water retention behaviour of unsaturated granular soils

Marius Milatz [a,*], Tom Törzs [a], Ehsan Nikooee [b,c], S. Majid Hassanizadeh [c], Jürgen Grabe [a]

[a] Institute of Geotechnical Engineering and Construction Management, Hamburg University of Technology (TUHH), Hamburg, Germany
[b] Department of Civil and Environmental Engineering, Shiraz University, Shiraz, Iran
[c] Department of Earth Sciences, Utrecht University, Utrecht, Netherlands

ARTICLE INFO

Article history:
Received 15 June 2017
Received in revised form 28 November 2017
Accepted 14 February 2018
Available online 19 February 2018

Keywords:
Soil-water retention behaviour
Transient effects
Suction stress
Granular soils
Matric suction measurement

ABSTRACT

In the present study, an experimental setup is presented and employed to examine the influence of rate of change of saturation on the transient water retention curves of granular soils with a low suction range. The results are evaluated and compared to existing theoretical approaches to model the non-equilibrium soil–water retention behaviour as well as to experimental findings from other researchers. Furthermore, suction stress characteristic curves under non-equilibrium conditions are obtained. Finally, the importance and the application of the results in hydro-mechanical modelling of unsaturated soils are discussed.

© 2018 Elsevier Ltd. All rights reserved.

1. Introduction

1.1. Investigation of the soil-water characteristic curve

The experimental investigation of the soil–water characteristic curve (SWCC) or water-retention curve (WRC) is of great importance in soil science, soil mechanics and hydrology. This relationship between capillary pressure p_c or matric suction s and volumetric water content θ or degree of saturation S_r represents a key function for the modelling of the hydro-mechanical behaviour of porous media such as soils in the unsaturated state.

The SWCC is known to experience hysteresis and a multitude of scanning-paths on drying and wetting cycles between full saturation ($S_r = 1$) and the so-called irreducible saturation S_{irr}, as depicted in Fig. 1. Another phenomenon is the influence of air entrapment which occurs during an imbibition. The imbibition paths do not reach full saturation and they will have a difference ΔS_r due to entrapped air.

The hysteresis phenomenon is due to various microscopic effects during the flow of pore water through the pore space; such as contact angle changes upon drying and wetting paths, the bottle neck effect, as well as air entrapment.[1] The macroscopic manifestation of these effects is the measurable SWCC with its highly non-linear behaviour and "hydraulic memory", i.e. path-dependence on hydraulic history.

Several methods have been developed for the experimental investigation of the SWCC in the laboratory.[2] These methods are characterised by different ranges and control accuracies of soil suction and are used for suction control in the measurement of SWCC or in mechanical testing of unsaturated soils. For the control of very high suction levels up to several megapascals in fine grained cohesive soils, methods, such as the osmotic technique[3] or the water vapour method, have been developed. In order to control medium to low suction levels relevant for granular soils, however, different methods are needed. One example is the axis translation method,[4] where suction $s = u_a - u_w$ is controlled by independent application of pore air pressure u_a and pore water pressure u_w. Other examples are the vacuum method, where suction is applied as underpressure, and the hanging water column method, where suction corresponds to negative pore water pressure and is applied by a negative water head.[2] Besides the control of suction, in many cases, accurate suction measurements are desirable. For this purpose, different instruments, such as tensiometers, can be employed. A benchmark for different measurement and control methods for suction has been published by Tarantino et al.[5] In most cases, the mentioned methods have been used for the determination of primary drainage paths of the soil. Generally, SWCC-measurement is a time consuming task. Therefore, only few data on the hydraulic response of unsaturated granular soils to higher order drying–wetting cycles is available.

* Corresponding author.
E-mail address: marius.milatz@tuhh.de (M. Milatz).

https://doi.org/10.1016/j.gete.2018.02.003
2352-3808/© 2018 Elsevier Ltd. All rights reserved.

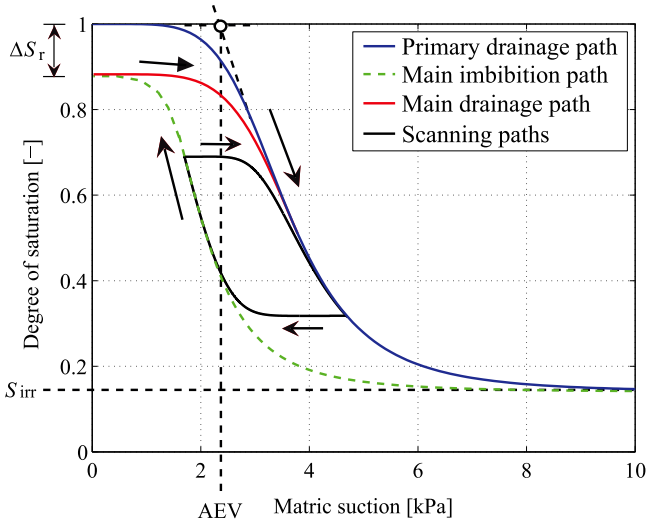

Fig. 1. Idealised hysteretic soil–water characteristic curve of a sandy soil with primary drainage, main imbibition, main drainage paths and different scanning paths.

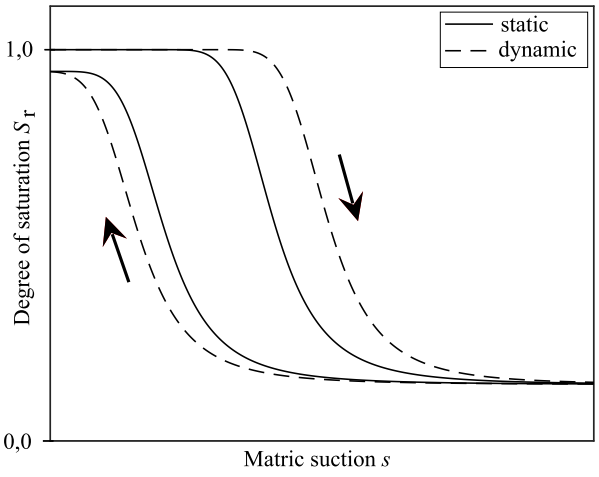

Fig. 2. Idealised static and dynamic soil–water characteristic curves of a sandy soil for primary drainage and main imbibition.

1.2. Transient effects and dynamic SWCCs

Different researchers have demonstrated experimentally that the SWCC obtained under transient conditions differs from an equilibrium SWCC, measured with one of the methods mentioned above. By applying sudden large changes in boundary conditions, many authors showed that "dynamic" SWCCs are obtained. Herein the primary and main drainage, as well as main wetting paths deviate from the equilibrium SWCCs as depicted in the schematic illustration in Fig. 2. A brief review of such studies will be given below.

For higher flow rates, an overshooting of suction on drainage paths and an undershooting on wetting paths are found that decay over time and approach the equilibrium suction. Therefore, from a macroscopic point of view, the phenomenon of a "dynamic" SWCC appears to be a result of different hydraulic equilibration processes inside the unsaturated soil. Extensive reviews of this dynamic effect can be found in Refs. 6, 7.

Among the previously mentioned studies, several key studies, their test setup, as well as their considered hydraulic paths are summarised in Table 1. It can be seen that the research on transient effects in unsaturated flow behaviour and soil-water characteristics already started with the important work by Topp et al.[8] However, mainly the primary hydraulic paths, especially for the drainage-case, have been studied so far. An exception can be seen in the recent work by Zhuang[16] who also evaluated the transient effects for scanning drainage paths. Therefore, very limited knowledge on non-equilibrium soil-water retention behaviour during different cycles of drainage and imbibition, including scanning paths, is available.

In Ref. 8, the drying SWCC of a sandy soil was determined under three different conditions: (a) static experiment, i.e. under equilibrium condition, (b) steady-state flow, and (c) unsteady-state flow. They noticed that the steady-state results are rather similar to those of equilibrium condition, whereas the resulting SWCCs of unsteady-state flow are different. It was observed that at a certain matric suction, the higher the flow rate is, the higher the degree of saturation would be.

The presence of disconnected pendular rings has been indicated as one of the possible reasons behind the difference between equilibrium and transient SWCC curves.[8,9] The strong influence of rate of change of saturation $\frac{\partial S_r}{\partial t}$ on the changes in SWCC under transient conditions has been pointed to by several researchers, e.g., Vachaud et al.[10] and Wanna-Etyem.[17] Further, soil type and consequently pore and grain size distribution are recognised to influence dynamic effects. However, there is yet not much consensus on the way soil texture and type influence the resulting dynamic curves. Wanna-Etyem[17] investigated the dynamic effects through several experiments on fine sand, dune sand, loamy sand and clay loam. It was observed that in the coarse-grained soils, dynamic effects are more pronounced than in the fine-grained soils. Wildenschild et al.[18] investigated dynamic effects through single and multi-step outflow experiments. Their investigated soil types included a sandy soil (88.6% sand, 9.4% silt, 2% clay) and a fine sandy loam (63.2% sand, 27.5% silt, 9.3% clay). They observed noticeable dynamic effects in the sandy soil while in the finer grained soil, they did not observe any dynamic effect. In contrast to these results, Camps-Roach et al.[19] have reported higher dynamic effects in finer textured soils. The reasons behind this discrepancy can root in several phenomena which influence dynamic effects. Having thought of faster possible equilibrium in coarse-grained soils, Smiles et al.[9] stated that the dynamic effects should increase by a decrease of larger pores within the pore size distribution. On the other hand, Wildenschild et al.[18] pointed to the sudden decrease in permeability after the air entry in uniformly grained soils which can result in the slower arrival at the equilibrium and more pronounced dynamic effects. Therefore, the value of permeability at different saturation levels as compared to the permeability in finer textured soils and the porous structure of soils can play an important role in the observed dynamic effects. Regardless of the mechanism (permeability or pore structure) higher water entrapment can lead to more noticeable dynamic effects.

Various mechanisms as a possible cause of dynamic effects have been discussed by Hassanizadeh et al.[6] and Nikooee et al.[20] Among all proposed mechanisms, the effect of air entrapment (especially in the pores adjacent to the boundary of the sample) can partly be attributed to experimental limitations and artefacts. In fact, the presence of a highly hydrophilic membrane at the outlet of an experiment can contribute to highly localised water drainage nearby and pore water blockage close to the boundary. Therefore, other mechanisms such as presence of heterogeneities rather than air entrapment, which are of more relevance to field conditions, may govern the dynamic effect at larger scales. Camps-Roach et al.[19] have considered pore water and air entrapment as less important as flow rate dependency of contact angle, with the latter being of key importance in observed dynamic effects. This brief discussion of literature reveals the importance of dynamic

Table 1
Selected previous studies on transient soil–water characteristics from literature.

Reference	Test setup	Studied hydraulic path
Topp et al.[8]	Rectangular soil specimen	Primary drainage
Smiles et al.[9]	Horizontal soil column	Drying and wetting
Vachaud et al.[10]	Vertical soil column	Primary drainage
Stauffer[11]	Vertical soil column	Primary drainage
Manthey[12]	Vertical soil column	Primary drainage
Bottero et al.[13]	Vertical soil column	Primary/main drainage/main imbibition
Das and Mirzaei[14]	Vertical soil column	Primary drainage
Mirzaei and Das[15]	Vertical soil column	Primary drainage/main imbibition
Zhuang[16]	"Small-volume unsaturated sand sample"	Primary/main/scanning drainage

soil-water characteristic curves in various hydraulic paths including scanning curves. However, the governing phenomena, which influence them, are all yet to be further studied due to our lack of understanding and comprehensive experimental observations.

1.3. Theoretical framework for dynamic SWCCs

Hassanizadeh and Gray[21] used a macro-scale thermodynamic framework for multiphase porous media consisting of upscaled balance laws for phases and interfaces as well as second law of thermodynamics. They proposed the following linearised equation to provide a relationship among the wetting and nonwetting fluid phase pressures and capillary pressure:

$$\frac{D^s s^w}{Dt} = -\frac{1}{\tau}\left[(p^n - p^w) - p_c\right] \tag{1}$$

where p^n and p^w denote nonwetting and wetting phase pressures, respectively, p_c is capillary pressure (matric suction) under static equilibrium conditions, and τ is a material parameter. Hassanizadeh and Gray[22] suggested that the material derivative $\frac{D^s s^w}{Dt}$ which is based on the solid phase motion can be substituted with its approximation, the time derivative of degree of saturation $\frac{\partial S_r}{\partial t}$, which would result in:

$$\left(p^n - p^w\right) - p_c = -\tau \frac{\partial S_r}{\partial t}. \tag{2}$$

According to Eq. (2), the so-called dynamic capillarity coefficient τ controls the speed of an equilibration process between the fluid pressure difference $(p^n - p^w)$ and the static capillary pressure p_c. For static equilibrium with $\frac{\partial S_r}{\partial t} = 0$, the left-hand side of Eq. (2) will be zero because the difference in pressures equals the capillary pressure.

For the coefficient τ, empirical formulae have been presented in the literature such as that of Stauffer[11]:

$$\tau = \left(\frac{0.1\varepsilon\mu}{k\lambda}\right)\left(\frac{P_e}{\rho g}\right)^2 \tag{3}$$

where μ specifies the fluid viscosity, ε is porosity, k denotes the hydraulic conductivity under saturated condition, P_e is the air entry pressure, and λ represents the Brooks and Corey-parameter also known as pore size distribution index.[23] ρ is the wetting fluid density and g is gravity.

Several studies have investigated the functional relationship of the dynamic capillarity coefficient and considered it to be complicated, and potentially hysteretic, i.e. being a function of saturation and matric suction both.[24,25] Furthermore, various functional dependencies have been proposed for this coefficient. Some have proposed it to be dependent also on other variables than simply saturation and suction, for instance on the rate of change of saturation, and specific fluid–fluid interfacial area.[25]

In order to investigate in more detail the whole representation of dynamic soil-water characteristic curves, a setup is needed for measuring water retention properties during different hysteretic cycles and in a systematic way for various flow rates. Such a device can later also facilitate studying the effect of soil type on dynamic soil-water characteristic curves. This study, therefore, introduces an experimental setup for investigating the dynamic soil-water characteristic curves during different hydraulic cycles. From the obtained data, the dynamic effect is quantified through calculating the dynamic capillarity coefficient τ. Furthermore, we discuss the importance of non-equilibrium effects on hydro-mechanical behaviour of unsaturated soils through the determination of non-equilibrium suction stress characteristic curves based on the obtained experimental data.

2. Experimental investigation of transient soil-water characteristic curves

2.1. Experimental method and test setup

With the original focus on the investigation of hysteretic drying–wetting paths of granular soils, a pore water volume-controlled experimental method has been developed. Contrary to conventional methods for the measurement of the SWCC, matric suction is not controlled but measured. The test is performed by imposing the pore water volume change while capillary pressure or matric suction is measured as a response.

An earlier version of the method was presented in Refs. 26, 27 to study the hysteretic SWCC of a medium coarse-grained sand and then it was further refined to study hydro-mechanical coupling and capillary collapse in sand due to drying and wetting cycles.[28]

The setup is based on a simple shear apparatus for the investigation of unsaturated sandy soils presented in Ref. 29. For the hydraulic tests presented in this contribution, the simple shear device was modified to be used as an oedometric cell with an either displacement- or force-controlled axial loading piston, a pore water pressure volume controller (manufactured by GDS Instruments Ltd, London, UK) and a topcap-tensiometer (T5 Laboratory Tensiometer, manufactured by UMS GmbH, Munich, Germany). The latter has been implemented into the loading piston to measure matric suction in the middle of the cylindrical soil specimen. A photograph of the setup is shown in Fig. 3. A schematic cross section, also illustrating the testing procedure and its boundary conditions, is depicted in Fig. 4.

The loading piston allows to apply axial stress to cylindrical soil specimens with a diameter of 50 mm and a height of ca. 20 mm. At the same time the porous ceramic tip of the topcap-tensiometer, installed in the middle of the loading piston, is pushed centrically into the middle of the soil specimen. Due to this position of the tensiometer tip and the small volume of the soil specimen, the suction measurement is assumed to be representative. A Linear Variable Differential Transformer (LVDT) allows to measure changes of specimen height with an accuracy of ± 0.005 mm. An accurate measurement of specimen height is important for the knowledge of pore space, needed to calculate the specimen's degree of saturation during the whole experiment.

The topcap-tensiometer is used to measure the capillary pressure inside the specimen. In order to prevent the build-up of excess

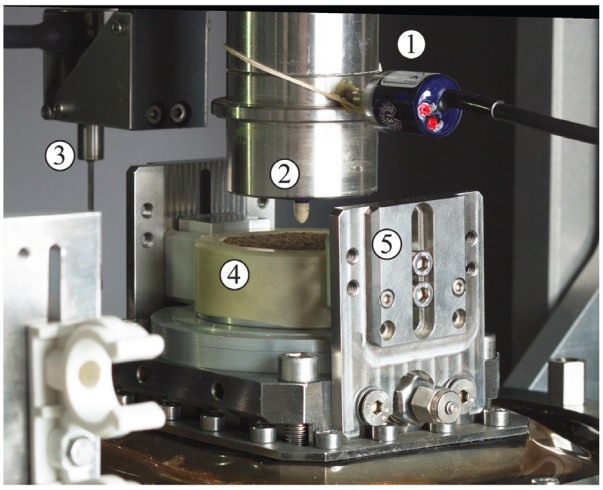

Fig. 3. The setup for the investigation of hysteretic soil–water retention curves of granular soils: ① T5 laboratory tensiometer, ② Loading piston with pointy ceramic tensiometer tip, ③ LVDT, ④ Cylindrical sand specimen in aluminium ring and latex membrane, ⑤ Membrane holder (for specimen preparation only).

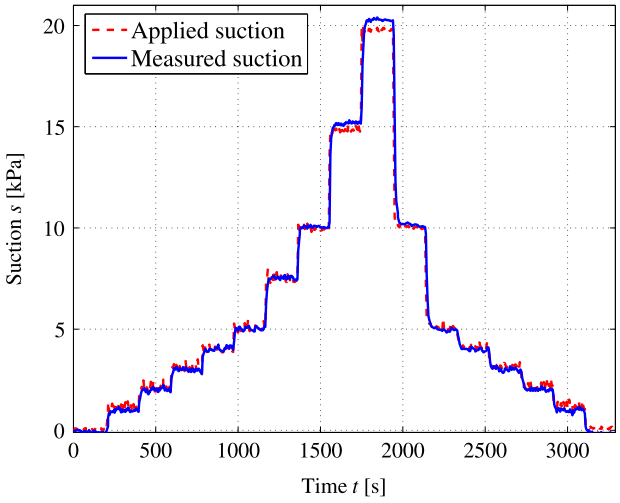

Fig. 5. Response- and accuracy-check of the topcap-tensiometer after its preparation and filling with de-ionised de-aired water.

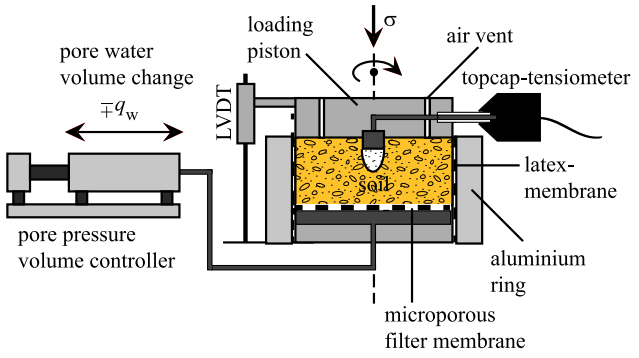

Fig. 4. Schematic cross section of the test setup and applied mechanical and hydraulic boundary conditions.

pore air pressure, the loading piston is equipped with air vents (see Fig. 4). Therefore, in the current test setup, the specimen top is subjected to atmospheric air pressure u_{atm}, and capillary pressure or matric suction, as measured by the topcap-tensiometer, is assumed to be equal to negative pore water pressure, i.e. $p_c = s = -u_w$ with $u_a = u_{\text{atm}} = 0$. In a possible enhanced setup for future tests, the non-wetting phase pressure could also be measured. For this purpose a second pressure transducer, e.g. using a hydrophobic membrane, could be used.

To change the saturation of the initially fully saturated sand specimen, a pore water pressure volume controller (manufactured by GDS Instruments Ltd, London, UK) is used as a pump. The computer-controlled device, which is usually used for triaxial testing, allows to draw water out of, and inject it back into, the specimen with a resolution of 1 mm^3. The pressure volume controller is filled with de-aired water and the water supply tube is connected to the specimen base pedestal, from where the water is forced through a porous stone filter, covered by a hydrophilic 0.8-μm microporous membrane.[30] The membrane (manufactured by PALL Corp., USA) has an average air entry value of 83 kPa and prevents the breakthrough of air into the dewatering system. At the same time it guarantees a high flow rate due to its nominal permeability of $1.2 \cdot 10^{-6}$ m/s and its negligible average thickness of 0.23 mm. According to the manufacturer, the water flow is in the range of 88.2 – 352.8 ml/(min · cm^2) at a water pressure of 70 kPa. The applied volume change ΔV_w (negative for specimen drainage) is measured by the pressure volume controller and logged by the control computer and is used for the calculation of degree of saturation according to Eq. (4). The calculation of S_r takes into account the change of the specimen void ratio e due to changes in specimen height, i.e. specimen volume V.

$$S_r = 1 + \frac{\Delta V_w}{\frac{e}{1+e} V}. \tag{4}$$

The computer control of the pressure volume controller allows to program the applied pore water volume change with mathematical functions. Either a sudden (sawtooth-function), a linear, a triangular or a sinusoidal change of pore water volume can be applied over time leading to corresponding flow rates of pore water $q_w(t)$. Therefore, the setup is suited well to investigate the hysteretic nature of the SWCC for arbitrary hydraulic paths and additionally investigate transient effects by systematically applying different flow rates $q_w(t)$ or rates of change of degree of saturation $\frac{\partial S_r}{\partial t}$. Due to the phenomenon of cavitation of the water either inside the tensiometer or inside the volume pressure controller occurring at suctions of around 1 atmosphere ($\approx$ 100 kPa), the application of the presented method is limited to granular soils with a typical range of matric suction below 100 kPa.

2.2. Testing procedure and specimen preparation

Before a planned test series, the topcap-tensiometer is prepared for measurement. The tensiometer-corpus, including the pressure transducer, the steel topcap and the porous ceramic tip are filled with de-ionised de-aired water and are carefully assembled. In order to ensure a bubble-free filling of the tensiometer with water and correct sensor measurements, the tensiometer is checked for its response to an applied suction and for accuracy. For this purpose, the ceramic tip of the topcap tensiometer is connected to a water reservoir, in which a negative water pressure is applied with a vacuum control device (VS-pro, manufactured by UMS GmbH, Munich, Germany). The result of such a response- and accuracy-check is depicted in Fig. 5.

The results show a very small response time for the tensiometer and a very good accuracy for the applied suctions up to 10 kPa. For higher suctions, slight deviations occur between applied and measured suction, which can be neglected for the tested sandy soils with a low relevant suction domain.

Table 2
Basic soil properties of the two investigated sands.

CTB-sand						
ρ_s [kg/m^3]	e_{min} [−]	e_{max} [−]	d_{10} [mm]	d_{max} [mm]	C_u [−]	k_w [m/s]
2650	0.41	0.86	0.16	2.00	2.4	$2.6 \cdot 10^{-4}$
ISS0-sand						
ρ_s [kg/m^3]	e_{min} [−]	e_{max} [−]	d_{10} [mm]	d_{max} [mm]	C_u [−]	k_w [m/s]
2650	0.60	1.02	0.11	0.48	1.7	$1.2 \cdot 10^{-4}$

ρ_s: grain density.
e_{min}/e_{max}: minimum/maximum void ratio.
d_{10}: grain diameter at 10% passing.
d_{max}: maximum grain diameter.
C_u: uniformity index.
k_w: hydraulic conductivity (Hazen formula).

Before each test, the base pedestal is assembled in a bath of de-aired and de-ionised water. The assembly consists of the connection of the dewatering tubes leading to the water pressure volume controller, also filled with de-aired de-ionised water, the clamping of the microporous filter membrane as well as the tightening of a latex membrane over the specimen-containing aluminium cylinder. The latex membrane is held in position by membrane holders which are removed after docking of the loading piston to the specimen top. The main purpose of the latex membrane is to seal the specimen in the modular specimen holder and prevent a leakage of pore water. Furthermore, it helps to reduce evaporation which is generally assumed to be negligible due to the narrow geometry of the air vents in the loading topcap. All tube connections as well as the porous sinter metal filter underneath the filter membrane are flushed with de-aired water in order to avoid the entrapment of air bubbles in the dewatering system.

Finally, the sand specimen is prepared by carefully pouring dry sand into the partially water-filled aluminium ring. During this procedure, care is taken that the water level is always on top of the sand surface to avoid occluded air bubbles. The sand is compacted to the desired initial specimen height by mixing with a small stick. After specimen preparation, the water-saturated base pedestal is placed in the testing device, then fixed and the loading piston is docked to the specimen top in a load-controlled procedure. During the docking, the ceramic tip of the topcap-tensiometer is carefully driven into the sand specimen. The docking procedure is finished when the axial load cell measures a docking force of 0.02 kN, corresponding to an initial axial stress of 10 kPa. This axial stress is kept constant until the subsequent testing steps are started. After the application of the docking stress, the membrane holders are dismounted and the latex membrane is rolled over the loading-piston and fixed with a rubber band.

The testing procedure generally consists of two stages. In the first stage, the initially water-saturated soil specimen is consolidated under an arbitrary axial stress σ, applied by the loading piston and kept constant throughout the whole experiment. After applying the selected stress, we wait until all settlements of the specimen top and possible excess pore water pressures, measured by the tensiometer in the middle of the specimen, have vanished. The second stage includes the hydraulic testing of the specimen and may be subdivided into further substages with different applied hydraulic paths. In order to avoid problems with a loss of hydraulic contact between the tensiometer and the pore water within the sand specimen, the lowest applied degree of saturation is limited to remain above $S_r = 0.3$ in the hydraulic test stages.

During the whole test, the axial displacement of the specimen top, i.e. the current specimen height, is exactly known. However, slight differences might occur in initial specimen height due to deviations resulting from specimen preparation. From the current specimen height, the updated void ratio as well as the updated degree of saturation are calculated for all test steps.

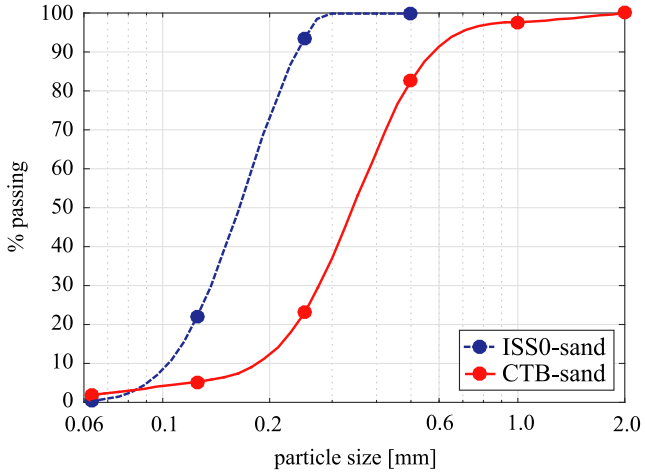

Fig. 6. Grain size distribution curves of the two investigated sands.

The tests presented in this contribution aim at the investigation of the influence of different rates of change of degree of saturation $\frac{\partial S_r}{\partial t}$ on the obtained hydraulic paths of the SWCC. For this purpose, constant inflow or outflow rates q_w are applied during the hydraulic stages by using the water pressure volume controller, which allows the evaluation of s-S_r data with also constant values of $\frac{\partial S_r}{\partial t}$. However, the values of $\frac{\partial S_r}{\partial t}$ have to be seen as average values for the individual hydraulic test stages because, technically speaking, they are only constant for the assumption of an unchanged void ratio. As the observed changes in void ratio are generally small, this assumption seems to be valid.

2.3. Tested material

Two different sands are considered in this study, in order to investigate their transient hydraulic behaviour. The investigated sands are a medium coarse-grained sand from the River Elbe in Hamburg, called CTB-sand,[27] and a fine-grained sand, called ISS0-sand, used for model tests in the soil mechanics laboratory at Hamburg University of Technology. Selected soil parameters are summarised in Table 2. The grain size distribution curves of the two sands are depicted in Fig. 6.

3. Laboratory tests and testing results

3.1. Hydraulic behaviour of medium coarse-grained sand

The hydraulic tests on CTB-sand were originally performed with the focus on the investigation of the hysteresis phenomenon and the scanning paths of the SWCC of this medium coarse-grained

Table 3
Hydraulic boundary conditions for the tests on CTB-sand.

Test Nr.	Applied q_w [mm^3/s]	Corresponding $\frac{\partial S_r}{\partial t}$ [1/s]
1	1.00	$\mp 7.29 \cdot 10^{-5}$
2	10.0	$\mp 7.41 \cdot 10^{-4}$

sand.[26,31] With the presented setup, different hydraulic histories in the form of varying drying–wetting paths were applied to the soil specimens. One of the test series, reported in this contribution, focuses on the influence of different flow rates on the measured hydraulic paths.

In the consolidation stage, the two sand specimens are loaded to an axial stress of 50 kPa, which is kept constant for the subsequent hydraulic test stages. A void ratio of $e_0 = 0.58$ is reached for both specimens at the beginning of the hydraulic test stages, which allows to assume equal starting conditions for the two specimens with respect to density. The hydraulic stages start with a primary drainage of the initially saturated sand, where S_r is reduced to 0.3. In the next step, two wetting–drying cycles with $0.3 \leq S_r \leq 1.0$ are followed by flushing the same pore water volume into and out of the specimen that has been removed in the primary drainage step. This procedure leads to a first imbibition path, followed by a main drying path and another imbibition path as well as one final main drying path. The hydraulic boundary conditions for the two specimens (the applied flow rates and the corresponding rates of degree of saturation change) are compared in Table 3.

To compare the applied flow rates to real flow events, they can be transformed into equivalent rainfall intensities of 44 and 440 mm/d. While the low value is realistic for a light rain event, the high value corresponds to heavy rain. It has to be emphasised however, that under natural conditions, very high rainfall intensities frequently only appear as peak values without being constant over a long period of time as in our experiments. However, besides the interpretation as a rainfall event, the applied higher flow rates could also represent the infiltration or exfiltration rate due to a quick flooding of the soil surface or a sudden lowering of the groundwater table.

The paths of s and S_r versus time, obtained from the two tests are shown in Fig. 7. The measured data are combined to construct SWCCs, shown in Fig. 8. For this data evaluation, a homogeneous distribution of s and S_r within the specimen volume is assumed, which may, however, be justified due to the small specimen height of only 20 mm.

The measured SWCCs show the typical hysteretic behaviour resulting from repeated drying and wetting. The applied pore water volume change does not consider the effect of air entrapment, when S_r is cycled between 0.3 and 1.0. Due to the occluded air after a first drainage, the pore water rises into the air vent holes in the topcap over the top of the sand specimen during the consecutive imbibition which can be noticed from the negative suction values measured by the tensiometer in Fig. 8. The negative suction values evolve linearly with increasing degree of saturation and represent a hydrostatic pore water pressure head on top of the specimen. However, the typical curve of the SWCC with a large slope $\frac{\partial s}{\partial S_r}$ around $s = 0$ during imbibition is very well captured by the data despite the enforced over-saturation.

After the first imbibition path, air entrapment (ΔS_r) can be derived from the curve of suction response and the point where suction becomes negative. The full degree of saturation is not reached again with the "real" S_r remaining at about 0.86 to 0.835. The amount of air entrapment ΔS_r increases from about 0.14 to 0.165 after the first wetting–drying cycle. In the second cycle of wetting and drying, it is slightly increased again for both specimens. It can be noticed that the two curves almost coincide despite the difference in the applied flow rates. This may indicate that the flow rate has no significant effect on the obtained SWCCs of the medium coarse-grained CTB-sand. As the curves lie very close to each other with some overlap, we conclude the value of the τ-parameter for this soil type to be negligibly small.

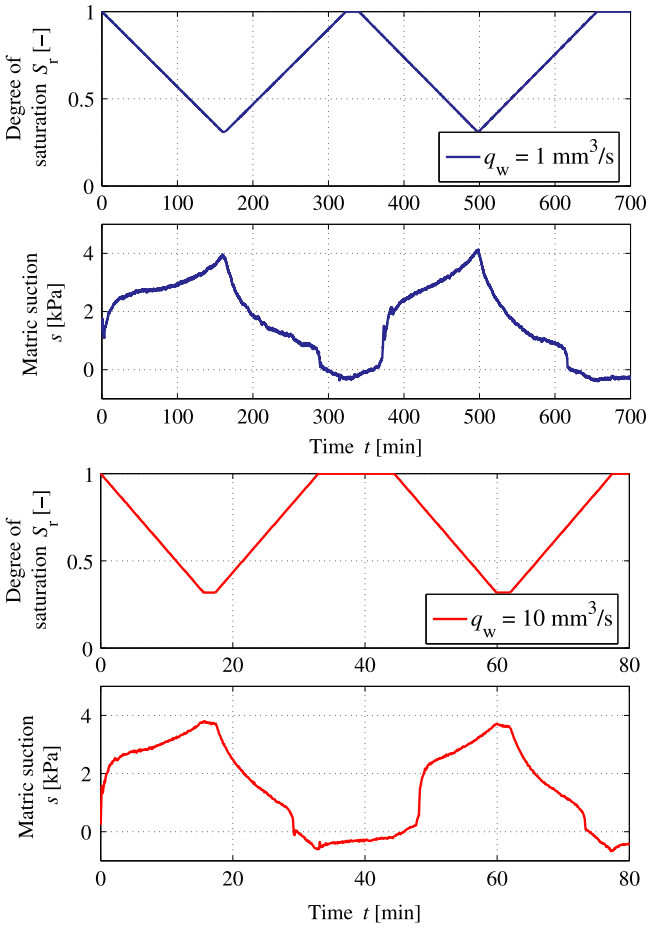

Fig. 7. Paths of measured matric suction s and degree of saturation S_r calculated from the applied pore water volume change for the two tests on coarse-grained CTB-sand. Note the difference in time scales.

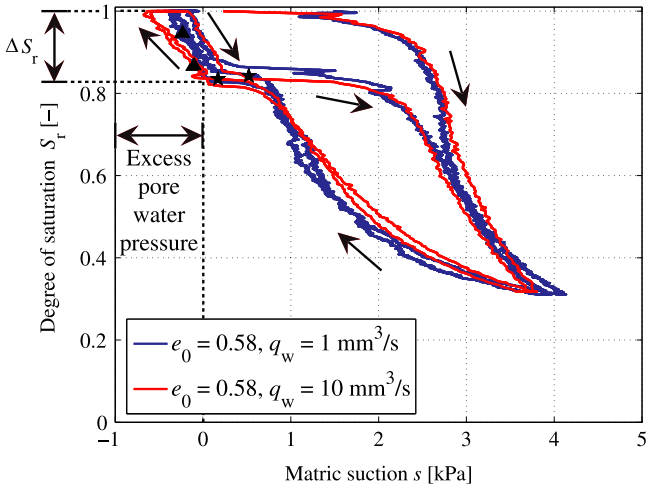

Fig. 8. Measured SWCCs of coarse-grained CTB-sand for the two varied flow rates.

Table 4
Testing stages and hydraulic boundary conditions for the tests on fine-grained ISS0-sand.

Test Nr.	Test stage	Applied q_w [mm^3/s]	Corresponding $\frac{\partial S_r}{\partial t}$ [1/s]
1	1: PD	0.25	$-1.45 \cdot 10^{-5}$
	2: I	0.25	$+1.45 \cdot 10^{-5}$
	3: CDW	0.25	$\mp 1.45 \cdot 10^{-5}$
	4: CDW	1.00	$\mp 5.79 \cdot 10^{-5}$
	5: CDW	2.50	$\mp 1.45 \cdot 10^{-4}$
2	1: PD	5.0	$-2.90 \cdot 10^{-4}$
	2: I	5.0	$+2.90 \cdot 10^{-4}$
	3: CDW	5.0	$\mp 2.90 \cdot 10^{-4}$
	4: CDW	7.5	$\mp 4.35 \cdot 10^{-4}$
	5: CDW	10.0	$\mp 5.80 \cdot 10^{-4}$

PD: Primary drainage, I: Imbibition, CDW: Cyclic drying–wetting.

3.2. Hydraulic behaviour of fine-grained sand

Two test series have been performed on the fine-grained ISS0-sand. For both specimens a void ratio of $e_0 = 0.8$ (medium dense packing) could be realised by careful preparation and similarly achieved compaction during the consolidation stage. In the consolidation stage, an axial stress of only 25 kPa is applied and kept constant throughout the whole experiment. The applied hydraulic paths consist of a primary drainage starting from $S_r = 1$, a following imbibition and different drying–wetting cycles. During all hydraulic stages, no significant change in the initial void ratio due to specimen volume change occurred.

The focus of the test series is placed on the flow rate effects. For both tests presented in this contribution, the primary drainage, the consecutive imbibition and first two drying–wetting cycles are performed with constant flow rate. Afterwards, two hydraulic test stages each with two drying–wetting cycles with an increased flow rate are applied. In the primary drainage path, the specimens are drained from $S_r = 1$ to $S_r = 0.4$. In the subsequent imbibition step, S_r is increased only to 0.8, in order to consider the effect of air entrapment without an over-saturation of the specimen. In the cyclic test stages, the upper limit of $S_r = 0.8$ is also taken into account and S_r is cycled between 0.8 and 0.5 in test 1 and between 0.8 and 0.6 in test 2. The applied boundary conditions of the two tests on ISS0-sand are compared for every test stage in Table 4.

The applied flow rates in ascending order reported in Table 4 correspond to rainfall intensities of 11, 44, 110, 220, 330 and 440 mm/d.

The time-series of obtained matric suction and degree of saturation for various stages of test 1 on ISS0-sand are depicted in Fig. 9. The transient SWCCs, obtained by combining the measured data of s and S_r, are depicted in Fig. 10. The data measured in the transient test is plotted together with data from an evaporation test using the HYPROP-laboratory test device (UMS GmbH/METER Group AG). In the HYPROP test, a cylindrical specimen with a diameter of 8 cm and a height of 5 cm and an initial void ratio of $e_0 = 0.8$ was subjected to free evaporation from its top surface, while suction was measured with two embedded tensiometers at different heights.[32,33] The degree of saturation is calculated over time from the mass loss of evaporated pore water measured with a laboratory balance. Due to the slow evaporation process, an equilibrium primary drainage path is obtained.

After the initial primary drainage, the following imbibition and first double drying–wetting path with a very slow flow rate of $q_{w,1} = 0.25$ mm^3/s, the flow rate is increased for the subsequent cyclic drying–wetting paths. The data, shown in Fig. 9, shows an increase in magnitude of suction response for higher flow rates.

A good agreement between the two primary drainage curves obtained for transient and equilibrium conditions (evaporation method) is obtained in the s-S_r-plane shown in Fig. 10. Without regard to the overshooting of suction around the air entry value from the transient test, the two primary drainage paths seem to be quite identical. From this it may be deduced that the transient curve with a flow rate of $q_{w,1} = 0.25$ mm^3/s corresponds to a static curve.

After the primary drainage and consecutive imbibition, the second main drainage path drifts to higher suctions and therefore crosses the primary drainage path. Normally, it would be expected that the second drainage path led asymptotically into the primary drainage path. This is a rather non-typical behaviour that cannot be explained by different flow rates because all described hydraulic paths are obtained for the same flow rate $q_{w,1} = 0.25$ mm^3/s. An attempt to explain this behaviour could be a developing inhomogeneity in the distribution of degree of saturation inside

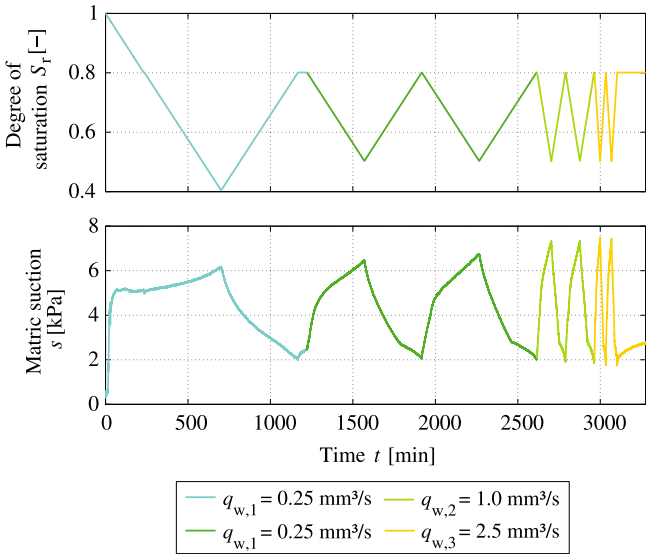

Fig. 9. Paths of measured matric suction s and degree of saturation S_r calculated from the applied pore water volume change for the first test on fine-grained ISS0-sand. The initial void ratio of each hydraulic test stage is $e_0 = 0.8$.

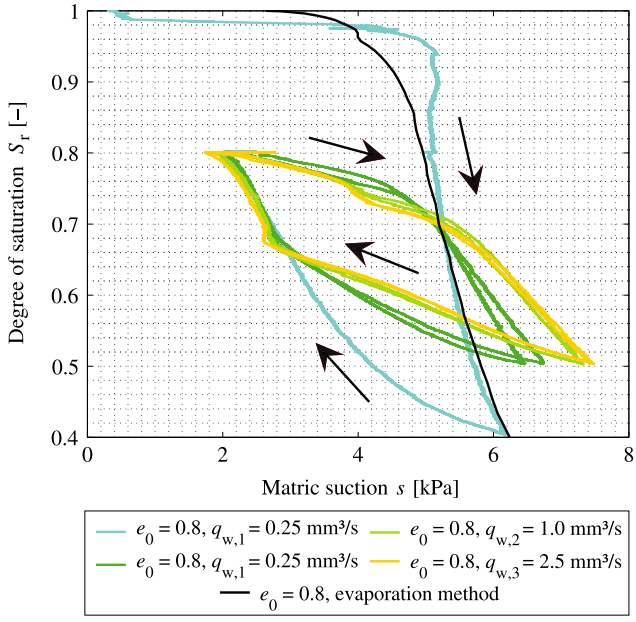

Fig. 10. Obtained transient SWCC for the first test on fine-grained ISS0-sand plotted together with an equilibrium primary drainage path from an evaporation test.

the specimen right after air entrapment. This would lead to a difference in local and global degree of saturation calculated from the pore water outflow. This effect would also cause the measured local suction values not to fit together with the calculated global degree of saturation. This phenomenon may also be accompanied by redistribution effects of pore water inside the specimen that promote an additional drift in the measured suction values visible in Fig. 9 after the first imbibition.

For the consecutive scanning drying curves with higher flow rates a drift farther in the direction of higher suction values can be noticed, which may reflect the transient effects that obviously also influence the scanning behaviour. However, the transient behaviour cannot be further described because all measured transient scanning curves start from a different hydraulic history of s and S_r and represent non-equilibrium curves. For an evaluation of the τ-parameter for the scanning curves according to Eq. (2), equilibrium-data with the same starting point within the s-S_r-plane would be needed. After the primary drainage and imbibition, the consecutive wetting curves show the typical behaviour of hydraulic history by running again into the previous main imbibition path.

Other evidence of non-equilibrium effects can be noticed from the s- and S_r-data close to the end of the test in Fig. 9. After the end of the last imbibition, the measurement of matric suction is continued for some time, showing an asymptotic increase of about 1 kPa, while the global degree of saturation remains at the applied value of 0.8. This may be an indication of redistribution effects within the specimen, leading to a drift towards the internal equilibrium suction and true equilibrium distribution of degree of saturation. In the applied test method, matric suction and degree of saturation are obtained as averaged values. Therefore, a possible redistribution of pore water over time and a change within a saturation distribution inside of the porous network can of course only be assumed.

The second test on ISS0-sand incorporates the same initial conditions with $e_0 = 0.8$ and $S_r = 1$. However, in the hydraulic test stages another concept is followed by applying generally higher flow rates compared to test 1. The measured data of S_r and s for test 2 are represented in Fig. 11. The SWCC from combined s-S_r-data is shown in Fig. 12.

Unlike the suction data from the first test, the cyclic drying–wetting paths from the second test with flow rates of $q_{w,1} = 5$ mm^3/s, $q_{w,2} = 7.5$ mm^3/s and $q_{w,3} = 10$ mm^3/s show only slight differences when compared to each other.

A difference between the first imbibition path and consecutive cyclic imbibition paths can be noticed which may be due to transient effects. However, the different cyclic hydraulic paths cannot be compared easily to each other with focus on the identification of dynamic effects, because their starting points, i.e. their hydraulic histories, differ slightly. Therefore, the dynamic effects cannot be described quantitatively, as already described for test 1. As a possible consequence of the higher flow rates, a slight settlement of the sand specimen is measured before the last cyclic drying–wetting stage, leading to a reduced void ratio of $e_0 = 0.79$.

The hydraulic test stages of the second test series generally differ from those of the first test series because of the higher applied flow rates. A comparison of the primary drainage paths of the tests 1 and 2 on ISS0-sand shows a higher suction response for the transient test with an initial drainage flow rate of $q_{w,1} = 5$ mm^3/s in test 2 compared to $q_{w,1} = 0.25$ mm^3/s in test 1. The two curves are shown in Fig. 13 and are also compared to the equilibrium primary drainage path for a void ratio of $e_0 = 0.8$, measured in the evaporation test mentioned above.

As these drainage paths experience the same initial conditions with same void ratio and same initial degree of saturation, the parameter τ may be evaluated. It can be easily computed from the

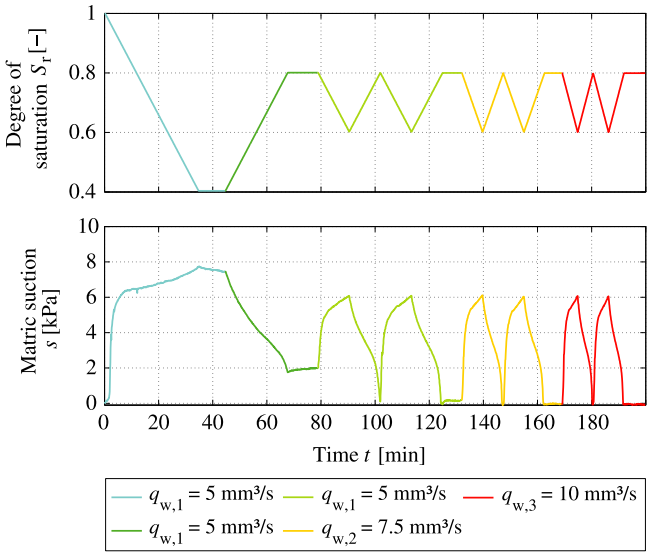

Fig. 11. Paths of measured matric suction s and degree of saturation S_r calculated from the applied pore water volume change for the second test on fine-grained ISS0-sand. The initial void ratio of each hydraulic test stage is $e_0 = 0.8$, except for the last stage where we have $e_0 = 0.79$.

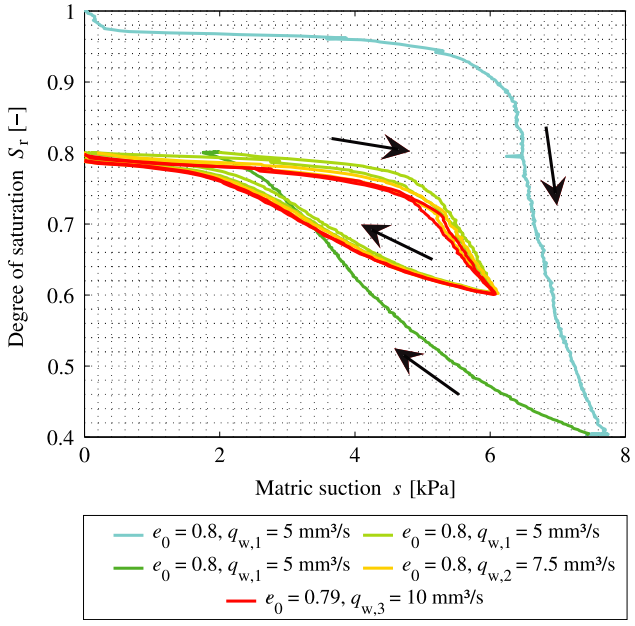

Fig. 12. Obtained transient SWCC for the second test on fine-grained ISS0-sand.

constant change rates of degree of saturation with time and the capillary pressure-difference between the primary drainage curves A and B as well as A and C using Eq. (2). In this evaluation, curve B is assumed to be equal to an equilibrium curve.

It is interesting to notice that the imbibition paths, also shown in Fig. 13, reach nearly the same suction value despite their varying starting points of suction and different flow rates. However, due to a lack of equilibrium imbibition data, τ cannot be evaluated for the imbibition paths.

The plots of the τ-parameter for primary drainage as a function of S_r- and s-values, based on data points shown by red markers in Fig. 13, are given in Fig. 14.

Despite the scatter of data, a linear relationship between τ and S_r or s can be fitted through all data points. It is given by Eqs. (5) and

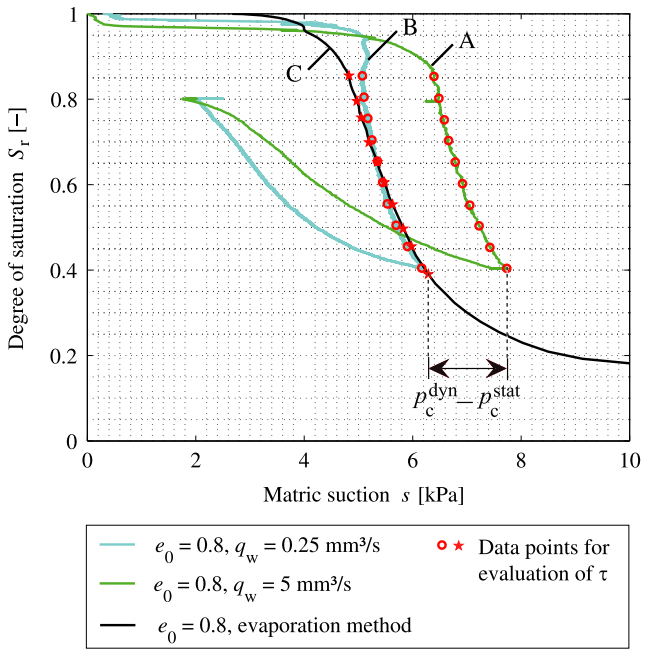

Fig. 13. Measured transient SWCCs of fine-grained ISS0-sand for primary drainage with consecutive imbibition (curves A and B) and comparison to an equilibrium primary drainage path from an evaporation test (curve C) for the calculation of the τ-parameter according to Eq. (2).

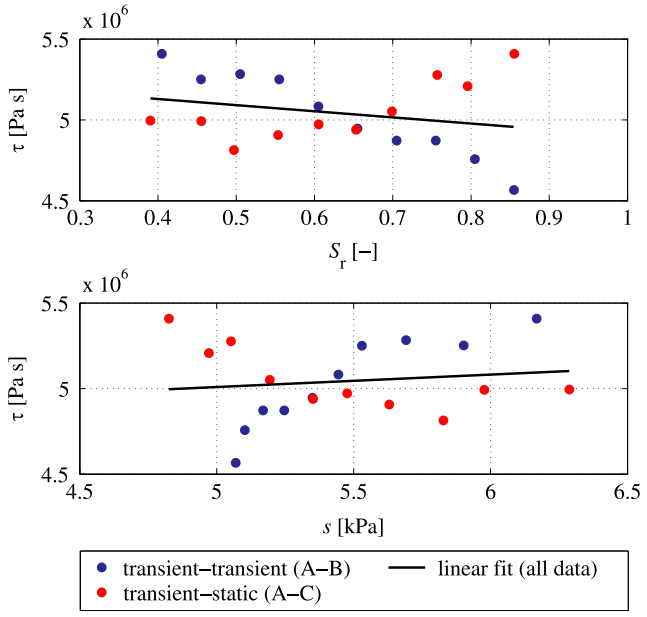

Fig. 14. Calculated τ parameter from test data as a function of S_r (top) and s (bottom) for the primary drainage path of the two transient SWCCs (curves A and B) and the equilibrium SWCC (curve C) of fine-grained ISS0-sand.

(6) valid for $0.39 \leq S_r \leq 0.86$ and $4.83 \leq s \leq 6.29$. The data show an increasing τ with decreasing degree of saturation or increasing matric suction. This is in accordance with some other findings in the literature. Other studies, such as the work by Bottero et al.,[13] Mirzaei and Das[15] and Zhuang,[16] also found the τ-parameter increasing with decreasing S_r.

$$\tau(S_r) = 5.2812 \cdot 10^6 - 0.3795 \cdot 10^6 \cdot S_r \quad [\text{Pa s}] \tag{5}$$

$$\tau(s) = 4.6453 \cdot 10^6 + 0.0728 \cdot 10^6 \cdot s \quad [\text{Pa s}]. \tag{6}$$

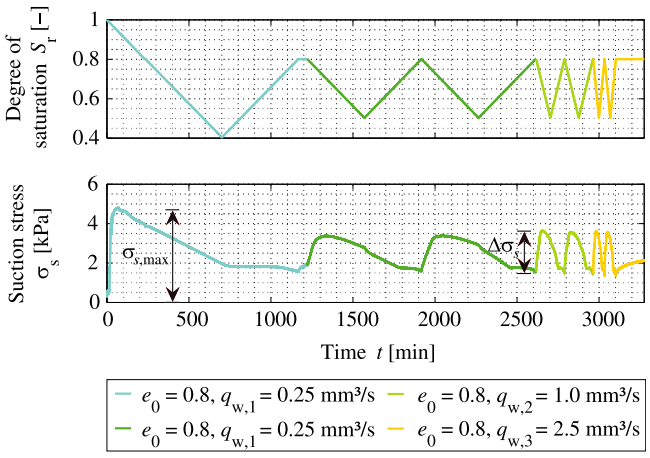

Fig. 15. Paths of degree of saturation S_r and calculated suction stress $\sigma_s = sS_e$ versus time for the first transient test series on fine-grained ISS0-sand.

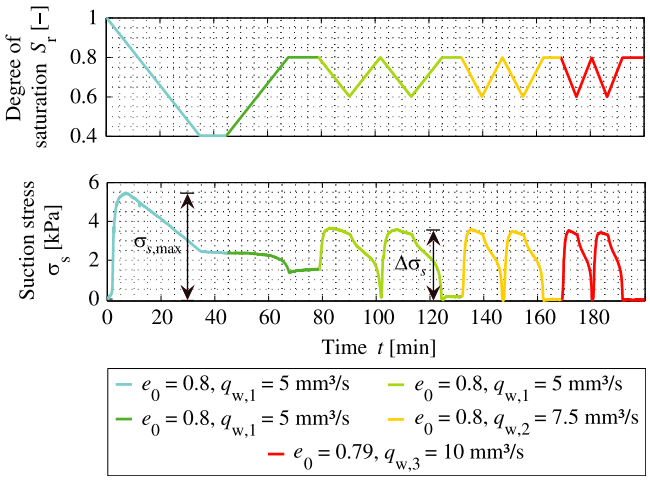

Fig. 16. Paths of degree of saturation S_r and calculated suction stress $\sigma_s = sS_e$ versus time for the second test series on fine-grained ISS0-sand.

3.3. Hydro-mechanical behaviour of fine-grained sand

Another practical significance of the presented findings can be seen in the impact of different flow or infiltration rates on the hydro-mechanical behaviour of unsaturated soils. The mechanical stress state and strength of unsaturated soils may also be influenced by different flow rates as occurring in nature for rain events with different rainfall intensities and corresponding infiltration rates. This would be relevant for the understanding of rainfall-induced slope failures. The influence of suction and degree of saturation on the effective stress state can be described by the suction stress concept.[34,35] Suction stress σ_s represents the influence of suction on the effective stress state and is given by Eq. (7).

$$\sigma_s = s\chi, \quad \text{with } \chi = S_e = \frac{S_r - S_{irr}}{1 - S_{irr}}. \tag{7}$$

To further emphasise this idea, the data from the hydraulic element tests on ISS0-sand are evaluated in terms of suction stress over time for different applied flow rates q_w. For the calculation of σ_s, a residual saturation $S_{irr} = 0.126$ is assumed in the formulation for effective saturation S_e. This value is reached asymptotically by the equilibrium primary drainage path, depicted in Fig. 13. The results of suction stress versus time are shown in Figs. 15 and 16.

The time series of calculated suction stress for the two tests on ISS0-sand also show the effect of hysteresis. For the higher

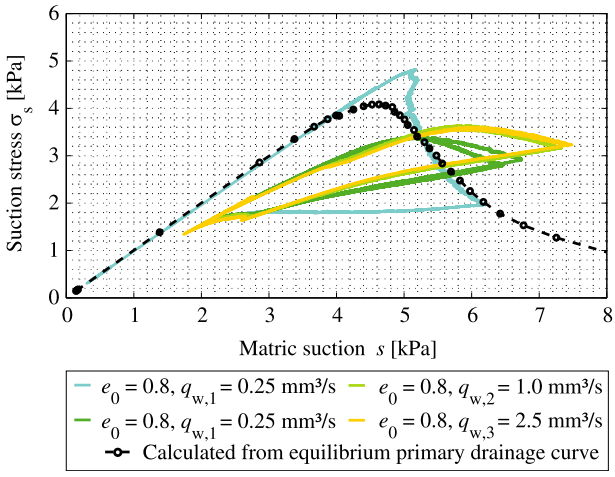

Fig. 17. Suction stress characteristic curves obtained from the first transient test series and from the equilibrium primary drainage path from the evaporation test on fine-grained ISS0-sand.

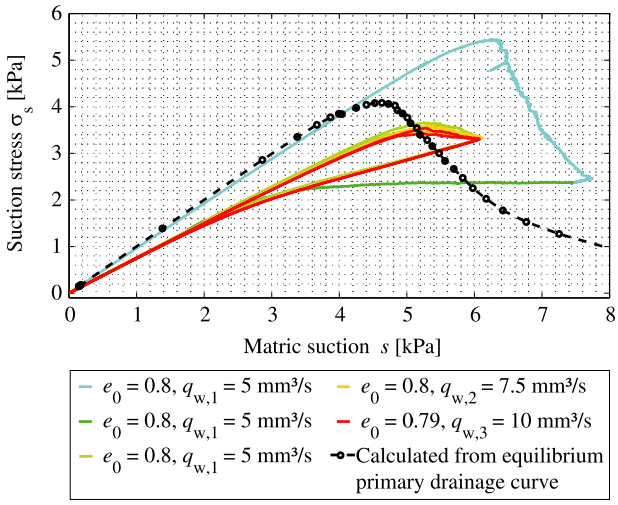

Fig. 18. Suction stress characteristic curves obtained from the second transient test series and from the equilibrium primary drainage path from the evaporation test on fine-grained ISS0-sand.

flow rates in test 2, the difference in suction stress for cyclic drying–wetting paths $\Delta\sigma_s$ is higher as compared to test 1, with $\Delta\sigma_{s,\text{test2}} \approx 3.45$ kPa, i.e. 63.6% of $\sigma_{s,\text{max,test2}}$, as compared to $\Delta\sigma_{s,\text{test1}} \approx 1.95$ kPa, i.e. 40.6% of $\sigma_{s,\text{max,test1}}$ in Figs. 15 and 16. Here, $\sigma_{s,\text{max}}$ indicates the maximum value of suction stress obtained for primary drainage in each test. This difference in the suction stress response of the two tests is an indication of a higher reduction of suction stress for higher flow rates. Additionally, in test 2 suction stress is reduced to approximately 0 kPa for the imbibition paths, which could represent an explanation for the observed settlements of the specimen before the last cycle (the reduction of void ratio from 0.80 to 0.79). This represents a link between the hydraulic and mechanical behaviours of unsaturated soil where changes in s and S_r may provoke capillary collapse.[28,36] Also, the above-mentioned effect of possible water redistribution is visible within the drift of suction stress at constant $S_r = 0.8$ for the last cycle in Fig. 15. This effect leads to generally lower suction stress for transient paths with an asymptotic drift to higher equilibrium suction stress at $\frac{\partial S_r}{\partial t} = 0$.

The above-mentioned hysteretic effect in suction stress becomes especially clear when suction stress is plotted versus matric suction in Figs. 17 and 18. These "suction stress characteristic curves" generally reveal higher suction stress levels for drying paths compared to wetting paths due to hysteresis of the SWCC. However, the development of suction stress on drying and wetting is non-linear with increasing or decreasing suction. Furthermore, the influence of dynamic effects can be seen especially within the results of the second test series in Fig. 18, when the transient suction stress curve for primary drainage is compared to the equilibrium curve. This transient suction stress response is generally higher than in the equilibrium state. Due to the low flow rate in the first transient test series the transient and equilibrium suction stress responses, shown in Fig. 17, are nearly identical, if the overshooting of suction stress around the air entry suction in the transient test is neglected.

Under natural conditions, cyclic wetting and drying paths with varying flow rates can occur for wet and dry weather periods with different intensities of rainfall and evaporation at the soil surface. Although the evaluated suction stress levels of the investigated ISS0-sand only account for a few kilopascals, their variability as a function of hydraulic history and flow rate may be significant for slope stability. Especially cyclic changes in suction stress and higher changes at higher flow rates may promote slope failure due to a loss of soil strength and redistribution of soil grains due to capillary collapse. However, this hypothesis needs further experimental testing.

4. Discussion and outlook

In this contribution, an experimental method for the investigation of arbitrary hydraulic paths of the SWCC of granular soils has been presented. The method is based on the direct application of flow rates of pore water and the measurement of the resulting suction response. The corresponding experiments, referred to as "hydraulic element tests", allow us to investigate the hysteretic nature of the SWCC upon cyclic drying–wetting paths as well as the influence of dynamic effects.

The main assumption of the hydraulic element test is a homogeneous distribution of capillary pressure or matric suction as well as degree of saturation within a small representative soil volume. This assumption may be justified because small specimens with a height of only 20 mm are tested with a centred suction measurement at the middle height of the specimens. However, deviations from a homogeneous distribution of capillary pressure and degree of saturation over the specimen may occur during an experiment due to boundary effects at the side walls of the specimen, as a result of increasing air entrapment or due to gravity. These effects may also lead to the observed indication of a redistribution of the water phase inside the specimen.

The principal findings of the presented research are the observed differences between the medium coarse-grained and the fine-grained sand with no significant dynamic effects in the transient drying–wetting paths of the coarse-grained sand. Mirzaei and Das[15] also show that the dynamic effects are more pronounced for finer-grained sands based on their column experiments. The results of Zhuang[16] show significant dynamic effects for main and scanning drainage of a fine-grained sand with a grain size distribution very similar to ISS0-sand used in this study. Her results also indicate a dependence of τ on S_r and an influence of hysteresis with determined values of $5 \cdot 10^4 \leq \tau \leq 3 \cdot 10^6$ Pa s. The order of magnitude of the τ-parameter for primary drainage found in this study is between $4.5 \cdot 10^6$ and $5.5 \cdot 10^6$ Pa s, which is in good agreement with the findings of Zhuang.[16] Despite some aberrations in the measured suction data from test series 1, the hydraulic element tests on the fine-grained ISS0-sand indicated

dynamic effects for all hydraulic paths of the SWCC, which represents another important finding. Also the scanning paths, only scarcely investigated in literature so far, appeared to be influenced by rate of change of degree of saturation with time. However, the value of τ could not be evaluated due to lack of corresponding equilibrium data for higher-order scanning paths.

To the best of our knowledge, this paper presents, for the first time, the experimental evidences of the influence of non-equilibrium retention behaviour of soil on its suction stress state. Due to difference in distributions of water inside the soil porous network at different water flow rates, one can expect different states of intergranular stress, i.e. different states of suction stress and alternatively effective stress. Nikooee et al.[20] have presented a formulation for the effective stress which accounts for the non-equilibrium effect (τ-term). However, still further non-equilibrium hydraulic as well as mechanical tests on unsaturated soils are needed to elucidate the role that non-equilibrium suction stress plays in the hydro-mechanical behaviour of unsaturated soils.

Further studies have been considered to employ the introduced experimental setup in order to obtain more data for the investigation of the transient soil–water characteristic curves as well as suction stress characteristic curves.

Last but not the least, an ongoing study has been considered by the authors where the same setup will be placed in a micro CT scanner to investigate the water distribution, homogeneity of saturation throughout the sample and trapped air and water clusters at different hydraulic states and their influence on the soil hydro-mechanical behaviour.

References

1. Bear J. In: *Hydraulics of Groundwater*. New York: Mc Graw-Hill; 1979; *Mc Graw-Hill Series in Water Resources and Environmental Eng*.
2. Vanapalli SK, Nicotera MV, Sharma RS. Axis translation and negative water column techniques for suction control. *Geotech Geol Eng*. 2008;26(6):645–660.
3. Cui C, Y , Delage P. Yielding and plastic behaviour of an unsaturated compacted silt. *Géotechnique*. 1996;46:291–311. http://dx.doi.org/10.1680/geot.1996.46.2.291.
4. Hilf JW. *An Investigation of Pore-Water Pressure in Compacted Cohesive Soils, Technical Memorandum No. 654*. (Dissertation), Colorado, USA: United State Department of the Interior Bureau of Reclamation, Design and Construction Devision Denver; 1956.
5. Tarantino A, Gallipoli D, Augarde C, De Gennaro V, Gomez R, Laloui L, Mancuso C, McCloskey G, Munoz J, Pereira JM, Peron H, Pisoni G, Romero E, Raveendiraraj A, Rojas JC, Toll D, Tombolato S, Wheeler S. Benchmark of experimental techniques for measuring and controlling suction. *Géotechnique*. 2011;61:303–312. http://dx.doi.org/10.1680/geot.2011.61.4.303.
6. Hassanizadeh SM, Celia MA, Dahle HK. Dynamic effect in the capillary pressure-saturation relationship and its impacts on unsaturated flow. *Vadose Zone J*. 2002;1:38–57. http://dx.doi.org/10.2136/vzj2002.3800.
7. Diamantopoulos E, Durner W. Dynamic nonequilibrium of water flow in porous media: A review. *Vadose Zone J*. 2012; 11. http://dx.doi.org/10.2136/vzj2011.0197.
8. Topp GC, Klute A, Peters DB. Comparison of water content-pressure head data obtained by equilibrium, steady-state, and unsteady-state methods. In: *Soil Science Society of America, Proceedings, Vol. 31*, 1967, pp. 312–314.
9. Smiles DE, Vachaud G, Vauclin M. A test of the uniqueness of the soil moisture characteristic during transient, non-hysteretic flow in a rigid soil. In: *Soil Science Society of America, Proceedings, Vol. 35*, 1971, pp. 535–539.
10. Vachaud G, Vauclin M, Wakil M. A study of the uniqueness of the soil moisture characteristic during desorption by vertical drainage. In: *Soil Science Society of America, Proceedings, Vol. 36*, 1972, pp. 531–532.
11. Stauffer F. Time dependence of the relations between capillary pressure, water content and conductivity during drainage of porous media. In: *Proceedings of the IAHR conference on scale effects in porous media, Thessaloniki, Greece*, 1978.
12. Manthey S. *Two-phase Flow Processes with Dynamic Effects in Porous Media - Parameter Estimation and Simulation*. (Dissertation), Institut für Wasserbau der Universität Stuttgart; 2006. Heft 157.
13. Bottero S, Hassanizadeh SM, Kleingeld PJ, Heimovaara TJ. Nonequilibrium capillarity effects in two-phase flow through porous media at different scales. *Water Resour Res*. 2011;47:1–11. http://dx.doi.org/10.1029/2011WR010887.
14. Das DB, Mirzaei M. Dynamic effects in capillary pressure relationships for two-phase flow in porous media: Experiments and numerical analyses. *AIChE J*. 2012;58:3891–3902.
15. Mirzaei M, Das DB. Experimental investigation of hysteretic dynamic effect in capillary pressure-saturation relationship for two-phase flow in porous media. *AIChE J*. 2013;59:3958–3974. http://dx.doi.org/10.1002/aic.14121.
16. Zhuang L. *Advanced Theories of Water Infiltration and Redistribution in Porous Media; Experimental Studies and Modeling*. (Ph.D. thesis), Utrecht, Netherlands: Utrecht University; 2017.
17. Wanna-Etyem C. *Static and Dynamic Water Content-Pressure Head Relations of Porous Media*. (Ph.D. thesis), Fort Collins, CO: Colorado State University; 1982.
18. Wildenschild D, Hopmans JW, Simunek J. Flow rate dependence of soil hydraulic characteristics. *Soil Sci Soc Am J*. 2001;65:35–48.
19. Camps-Roach G, O'Carroll DM, Newson TA, Sakaki T, Illangasekare TH. Experimental investigation of dynamic effects in capillary pressure: Grain size dependency and upscaling. *Water Resour Res*. 2010;46:W08544.
20. Nikooee E, Hassanizadeh SM, Habibagahi G. Mechanics of unsaturated soils: from equilibrium to transient conditions. In: *Proceedings of the Fifths Biot Conference on Poromechanics*, 2013, pp. 2049–2058.
21. Hassanizadeh SM, Gray WG. Mechanics and thermodynamics of multiphase flow in porous media including interphase boundaries. *Adv Water Resour*. 1990;13:169–186.
22. Hassanizadeh SM, Gray WG. Thermodynamic basis of capillary pressure in porous media. *Water Resour Res*. 1993;29:3389–3405.
23. Brooks RH, Corey AT. Hydraulic properties of porous medium. Hydrology Paper No. 3, (pp. Civil Engineering Department, Colorado State Univ., Fort Collins, Colorado), 1964.
24. Sakaki T, O'Carroll DM, Illangasekare TH. Direct quantification of dynamic effects in capillary pressure for drainage-wetting cycles. *Vadose Zone J*. 2010;9:424–437.
25. Joekar-Niasar V, Hassanizadeh SM. Effect of fluids properties on nonequilibrium capillarity effects: Dynamic pore-network modeling. *Int J Multiph Flow*. 2011;37:198–214.
26. Milatz M, An experimental method to study the drying-wetting behaviour of a sand. In: Z. Chen, C. Wei, D. Sun, & X. Xu (Eds.), *Proc. of 6th Asia-Pacific Conference on Unsaturated Soils (AP-UNSAT 2015), Guilin, China*, 2015, pp. 211–216.
27. Milatz M, Untersuchungen zum Einfluss der Kapillarität auf das hydraulisch-mechanische Verhalten von granularen Tragschichten für Verkehrswege. Dissertation. Veröffentlichungen des Instituts für Geotechnik und Baubetrieb der Technischen Universität Hamburg-Harburg, vol. 36 (in German), 2016.
28. Milatz M, Törzs T, Grabe J. Settlements in unsaturated granular soils induced by changes in saturation and suction. In: *Proc. of 3rd European Conference on Unsaturated Soils (E-UNSAT 2016), Paris, France*, 2016, http://dx.doi.org/10.1051/e3sconf/20160914009.
29. Milatz M, Grabe J. A new simple shear apparatus and testing method for unsaturated sands. *Geotech Test J*. 2015;38:9–22. http://dx.doi.org/10.1520/GTJ20140035.
30. Nishimura T, Koseki J, Fredlund DG, Rahardjo H. Microporous membrane technology for measurement of soil-water characteristic curve. *Geotech Test J*. 2012;35(1):1–8.
31. Törzs T, Experimental and numerical investigations on moisture transport in unsaturated soils. Masterthesis. Institute of Geotechnical Engineering and Construction Management, Hamburg University of Technology, 2015.
32. Peters A, Durner W. Simplified evaporation method for determining soil hydraulic properties. *J Hydrol*. 2008;356:147–162.
33. UMS 2017. HYPROP operation manual. UMS GmbH, Munich, Germany. URL http://www.ums-muc.de/assets-ums/009VP.pdf, (last time accessed on 11.09.17).
34. Lu N, Likos WJ. Suction stress characteristic curve for unsaturated soil. *J Geotech Environ Eng*. 2006;132(2):131–142.
35. Lu N, Godt JW, Wu DT. A closed-form equation for effective stress in unsaturated soil. *Water Resour Res*. 2010; 46.
36. Bruchon J-F, Pereira J-M, Vandamme M, Lenoir N, Delage P, Bornert M. Full 3d investigation and characterisation of capillary collapse of a loose unsaturated sand using x-ray ct. *Granular Matter*. 2013;15:783–800.